



This is a repository copy of *Accelerating growth of Sermilik Delta, Greenland (1987–2022), driven by increasing runoff.*

White Rose Research Online URL for this paper:

<https://eprints.whiterose.ac.uk/228532/>

Version: Published Version

Article:

Crick, R., Livingstone, S.J. orcid.org/0000-0002-7240-5037 and Sole, A.J. (2025) Accelerating growth of Sermilik Delta, Greenland (1987–2022), driven by increasing runoff. *Earth Surface Processes and Landforms*, 50 (8). e70116. ISSN 0197-9337

<https://doi.org/10.1002/esp.70116>

Reuse

This article is distributed under the terms of the Creative Commons Attribution (CC BY) licence. This licence allows you to distribute, remix, tweak, and build upon the work, even commercially, as long as you credit the authors for the original work. More information and the full terms of the licence here:

<https://creativecommons.org/licenses/>

Takedown

If you consider content in White Rose Research Online to be in breach of UK law, please notify us by emailing eprints@whiterose.ac.uk including the URL of the record and the reason for the withdrawal request.



eprints@whiterose.ac.uk
<https://eprints.whiterose.ac.uk/>

Accelerating growth of Sermilik Delta, Greenland (1987–2022), driven by increasing runoff

Rebecca Crick | Stephen J. Livingstone  | Andrew J. Sole

School of Geography and Planning, University of Sheffield, Sheffield, UK

Correspondence

Stephen J. Livingstone, School of Geography and Planning, University of Sheffield, Sheffield, S10 2TN, UK.

Email: s.j.livingstone@sheffield.ac.uk

Funding information

N/A.

Abstract

The Greenland ice sheet (GrIS) produces ~8% of the global suspended sediment delivered to the oceans and is the only Arctic region where deltas are advancing. However, understanding of the dynamics of sediment transfer from source-to-sink and the impact of variations in climate and ice sheet processes on sediment yields are uncertain. Here, we investigate controls governing the annual evolution of a proglacial fjord-head delta (Sermilik Delta) located on the southwest coast of Greenland from satellite-derived shorelines and modelled tides (1987–2022). Our results reveal delta progradation of ~26 km² from 1987 to 2022 (0.78 km² year⁻¹) with an accelerating trend controlled by meltwater runoff, including increases in the annual total and frequency of extreme events. The lack of correlation between delta growth and ice velocity, with the latter decreasing over the study period, indicates a readily accessible store of subglacial and proglacial sediment that meltwater can tap into. Expansion of the proglacial zone, which is inundated during high runoff providing a well-connected source of sediment, might explain the strengthened relationship between runoff and delta growth since 2010. We highlight the importance of tides on the morphology of proglacial deltas during low runoff, and the potential of using tidal model data to remove the tidal signal and isolate real changes in delta area.

KEYWORDS

Arctic, deltas, glacial meltwater runoff, Greenland ice sheet, progradation, sediment transport, shoreline-change

1 | INTRODUCTION

Ice sheets respond to climate by adjusting their spatial extent and flow dynamics, which modifies their ability to do geomorphic work and produce sediment (Jaeger & Koppes, 2016). Amplified anthropogenic warming of the Arctic (Dai et al., 2019; IPCC, 2021; Serreze & Barry, 2011) is causing the Greenland ice sheet (GrIS) to lose mass, making it one of the largest present-day contributors (Mouginot et al., 2019; Shepherd et al., 2020) to global mean sea level rise (Aschwanden et al., 2019; Goelzer et al., 2020). Mass loss is largely driven by surface melting and runoff and increased glacier flow (King et al., 2020), which promote the erosion and transfer of subglacial sediment into the proglacial and coastal environments (Cook et al., 2020; Hasholt et al., 2018; Koppes et al., 2015).

The GrIS is a significant supplier of sediments to the proglacial area and ocean (Bendixen et al., 2017; Hasholt et al., 2018; Overeem et al., 2017). It currently produces ~8% of modern suspended sediment output to the global ocean, with 80% of this fluvial sediment load concentrated within just 15% of its rivers (Overeem et al., 2017). While very few measurements of erosion rates beneath the GrIS exist, indirect observations from catchments with significant surface meltwater inputs and basal ice motion, suggest they closely resemble those measured at temperate alpine glaciers (Cowton et al., 2012; Herman et al., 2021; Overeem et al., 2017; Young et al., 2016). Meltwater production promotes glacial sliding, erosion and sediment transfer, but the relationship is strongly influenced by low-frequency high-magnitude flood events (e.g., Carrivick & Heckmann, 2017; Cook et al., 2020; Doyle et al., 2015), the availability of sediment and the

This is an open access article under the terms of the [Creative Commons Attribution](https://creativecommons.org/licenses/by/4.0/) License, which permits use, distribution and reproduction in any medium, provided the original work is properly cited.

© 2025 The Author(s). *Earth Surface Processes and Landforms* published by John Wiley & Sons Ltd.

seasonal evolution of the subglacial drainage system (e.g., Alley, 1992; Cowton et al., 2012; Swift et al., 2002; Swift et al., 2005). Thus, there is uncertainty regarding the spatial distribution of erosion beneath the GrlS, and whether the observed sediment flux represents the erosion product of a single year or includes additional remnants from previous years (Cowton et al., 2012).

Once sediment is evacuated from the subglacial environment, the proglacial foreland acts as a filter controlling the connectivity and flux of sediment transported from the ice margin to the ocean (Lane et al., 2017; Mancini et al., 2023; Orwin & Smart, 2004; Porter et al., 2019). This filtering process depends on the amount of sediment supplied and the sediment carrying capacity of the water and is influenced by various local factors such as topography, stream dynamics and paraglacial processes (Lane et al., 2017). Where proglacial rivers meet the ocean, sediment is deposited, typically in Gilbert-type deltas (Irrgang et al., 2022; Overeem et al., 2022). Greenland is the only Arctic region where deltas have advanced since the 1980s (Bendixen et al., 2017). Coastline mapping of 121 Greenlandic deltas showed that 75 of these deltas prograded at an average rate of 0.011 km² per year since the 1940s. This increased sediment flux might provide an opportunity for Greenland to become a global exporter of sand and aggregates (Bendixen et al., 2019), helping indigenous communities towards economic independence (Bendixen et al., 2019, 2022).

Deltas form the critical interface and transition zone between the land and ocean (Overeem et al., 2022): filtering sediment and nutrients (e.g., Rawlins et al., 2010), controlling the distribution of fluvially sourced carbon, acting as efficient sinks of inorganic and organic material (Smith et al., 2015) and modulating biogeochemical cycles (Hawkings et al., 2015, 2016; Hopwood et al., 2020; Meire et al., 2015). Greenlandic delta morphology is governed by the balance between sediment input from upstream (mainly ice sheet) processes and river discharge and downstream marine processes, such as tidal and wave action, that redistribute and export the sediment (Kroon

et al., 2011). Tidal dynamics in the coastal waters of Greenland are modulated by long, narrow fjords and an extensive shallow continental shelf (Richter et al., 2011).

Understanding how Greenlandic deltas and proglacial forelands respond to variations in climate and ice sheet processes is crucial to estimating future changes to the transport of freshwater, sediment, nutrients and heat that impact marine ecosystems (Hopwood et al., 2020). Mass loss from the GrlS is predicted to increase by 2100 (Goelzer et al., 2020). However, our understanding of glacial erosion and sediment transport processes, the timescales over which these processes operate, and their response to changing climate and glacier dynamics is uncertain. This is primarily due to the complexity of ice–water–sediment interactions (Cook et al., 2020; Savi et al., 2023) and the paucity of empirical data on the production and transfer of sediment from source-to-sink (Alley et al., 2019; Jaeger & Koppes, 2016). Other than the pioneering study of Bendixen et al. (2017), little work has focused on the sedimentary coasts of Greenland (e.g., Bendixen & Kroon, 2017; Kroon et al., 2011; Kroon et al., 2017; Nielsen, 1994; Pedersen et al., 2013).

This study aims to quantify environmental controls governing the morphodynamic evolution of the Sermilik Delta, a proglacial fjord-head delta situated within the topographically confined (3–4 km wide) Sermilik Fjord, located on the south-west coast of Greenland (Figure 1) (63°31'52.32"N, 50°45'20.48"W). The Sermilik Delta is fed by meltwater runoff from the Sermeq Glacier catchment. The Sermeq River delivers around a quarter of Greenland's total suspended sediment to the ocean (Overeem et al., 2017). This delta was selected as it prograded at an exceptional rate of 0.47 km² year⁻¹ between the 1980s and 2010s (Bendixen et al., 2017) making it the fastest growing delta in Greenland. In this study, we employ optical satellite imagery and modelled tide heights to quantify temporal changes in delta shoreline position and area between 1987 and 2022 to determine ice sheet and climate factors governing sediment transport and deposition.

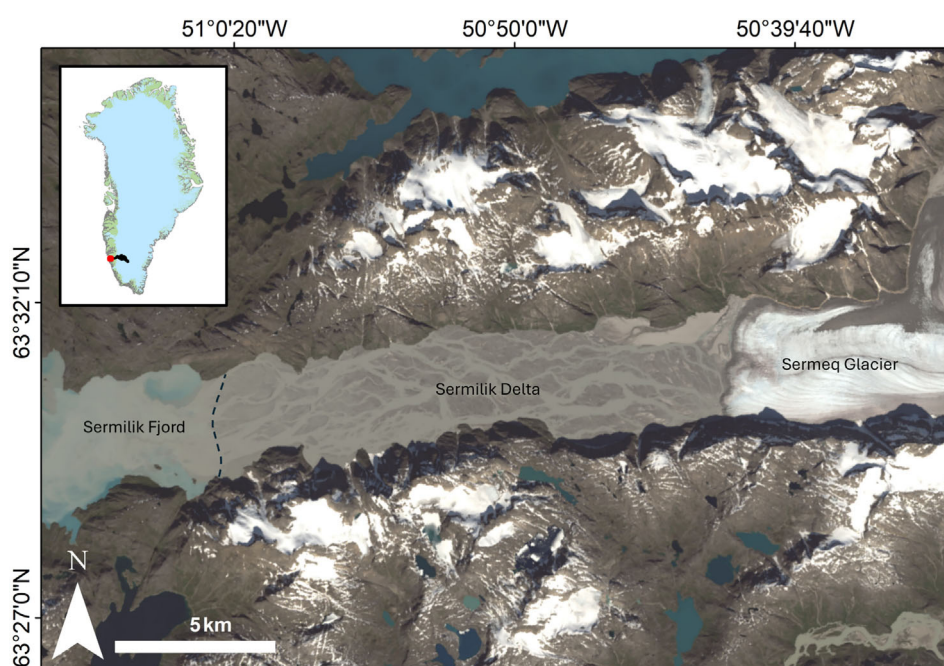


FIGURE 1 Location of the study area showing the Sermilik Delta located at the head of Sermilik Fjord, adjacent to Sermeq Glacier (right) in south-west Greenland (top left). The dashed black line represents an approximate delta shoreline. The black polygon on the inset map outlines the drainage basin area (7179 km²). Background image is a Landsat 9 true colour image (acquired on 13 August 2022).

2 | DATA AND METHODOLOGY

2.1 | Mapping delta area

To measure changes in the spatial extent of the Sermilik Delta, shorelines were mapped with satellite imagery processed in Google Earth Engine (GEE) and manually digitised using the GEE Digitisation Tool (GEEDiT) (Lea, 2018). Satellite images from Landsat 5, 7, 8 and 9 (30-m resolution) and Sentinel-2 (10-m resolution) were acquired between 1987 and 2022 to map delta area change at high temporal and spatial resolution. In addition to true colour images, the Short-Wave Infrared (SWIR) band (30-m resolution for Landsat and 20-m resolution for Sentinel-2) aided in the identification of the delta shoreline due to distinct differences in albedo between water and land (e.g., Figure 2b). Delta shoreline extent was delineated by interpolating straight lines between mouth bars rather than tracing distributary channels (e.g., Figure 2). This was effective at reducing variability in the delta area between each observation. To reduce uncertainty in mapping, islands (mouth bars) were included as part of the delta. Mapping was restricted to June to September to encompass the melt

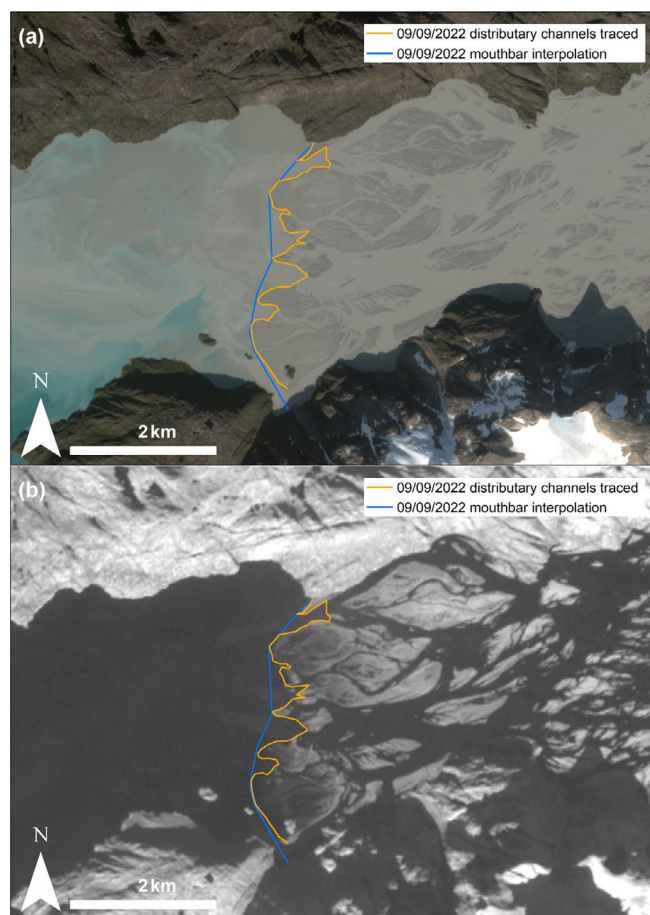


FIGURE 2 Examples of the identification of the delta extent. The land–water boundary was drawn where the shoreline could be identified. The orange line represents mapping distributary channels and mouth bars, and the blue line represents mapping straight lines between mouth bars. Island mouth bars are included as part of the delta extent. Background image (a) is a Sentinel-2 true colour image (acquired on 9 September 2022) and (b) is the Short-Wave Infrared (SWIR)-band 12 of the same image.

season and minimise the impact of snow, sea-ice and shadows from fjord valley walls (e.g., Figure 3b). Fluvial flooding of the delta plain also obscured the delta shoreline, making identification difficult for some images during the melt season (e.g., Figure 3a).

In total, 223 delta shorelines were mapped from 1987 to 2022. The mapped delta shorelines were exported from GEEDiT in vector format as separate shapefiles into ArcMap 10.7. To calculate the area of the delta, the outline of the fjord valley walls was manually delineated from a satellite image with a consistent landward baseline used as a reference, similar to Bendixen et al. (2017). The delta shoreline and fjord outline shapefiles were combined into a polygon for each delta front date in MATLAB in order to calculate the change in delta area.

2.2 | Delta area tidal correction

Tidal variation has a significant impact on the accuracy of mapped shoreline positions (Boak & Turner, 2005; Vos et al., 2023), particularly for deltas with shallow surface slopes. Figure 4a,b demonstrates the difference between a high and low tide from two consecutive images of Sermilik Delta, and Figure 4c illustrates the influence of the fluctuating tidal cycle on delta shoreline mapping from satellite imagery at a sub-annual temporal resolution. To mitigate the impact of tides, previous studies identified the high-waterline on the delta plain as the delta shoreline (Bendixen et al., 2017). In this study, we mapped delta shorelines from all suitable images and mitigated the effect of the tide on the position of the delta shoreline by using modelled tide height predictions at the time of image acquisition to implement a tidal correction.

2.3 | Tidal data

Modelled tidal data for the Sermilik Fjord study region were generated using the Greenland 1-km Tide Model (Gr1kmTM; Howard & Padman, 2021), available from the Arctic Data Centre. The Tide Model Driver version 2.5 (TMD) package (Erofeeva et al., 2020) was run in MATLAB, allowing modelled tidal phases to be generated for the study period. The Gr1kmTM is a barotropic ocean tide model on a polar stereographic grid with a resolution of 1×1 km. This high-resolution tidal model is well-suited for accurate tidal predictions in fjord environments. The Gr1kmTM consists of spatial grids of complex amplitude coefficients for sea surface height (relative to the seabed, i.e., ‘ocean tide’) and depth-integrated currents (‘volume transports’) for eight principal tidal constituents: four semi-diurnal constituents (M2, S2, K2 and N2) and four diurnal constituents (K1, O1, P1 and Q1). Tidal height predictions incorporating all harmonic constituents generated for grid cells within Sermilik Fjord were used as an approximation of the tidal signal and phase at the delta front. The tides in Sermilik Fjord are mixed semi-diurnal, with a predicted mean tidal range of ca. 2.6 m and a spring tidal range of ca. 3.8 m. Uncertainty in the modelled tidal output mainly stems from the dependence of tidal currents on water column thickness, which is poorly constrained in Sermilik Fjord. However, the modelled tidal range is consistent with observed tidal variations along the delta slope (see Figure 4), giving confidence in the model’s performance.

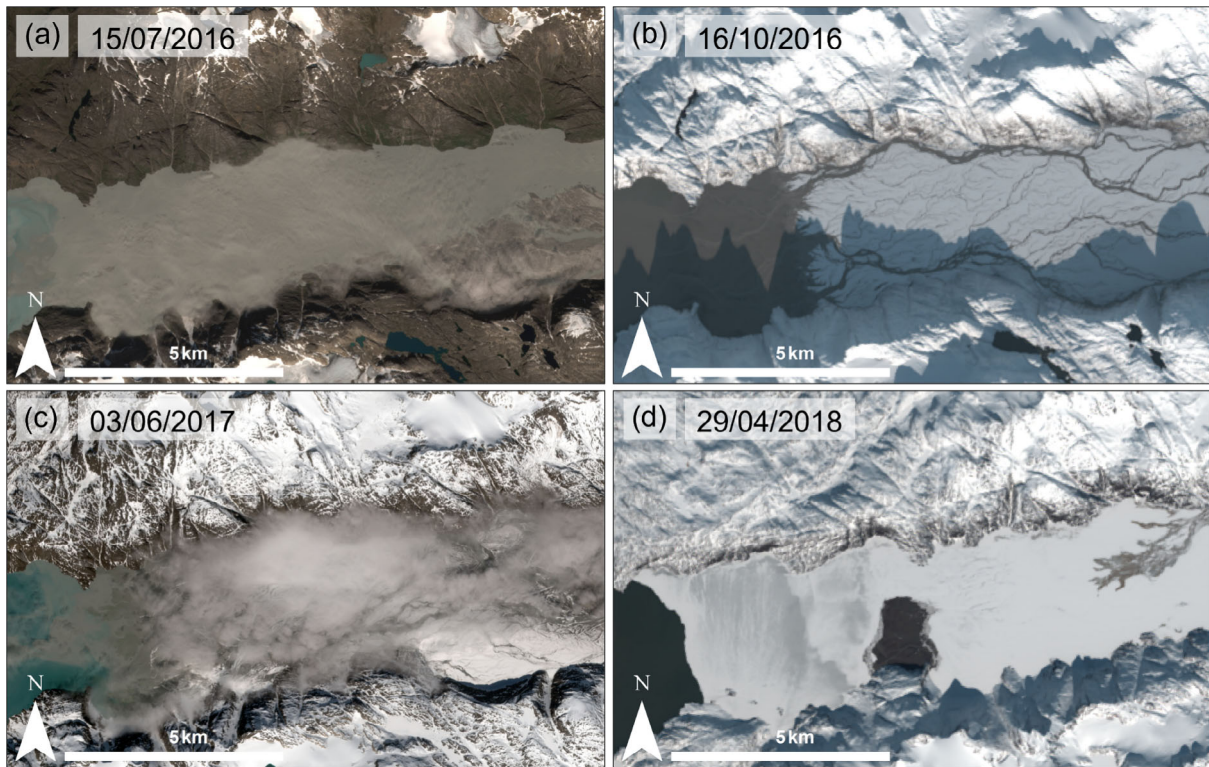


FIGURE 3 Examples of how shorelines can be difficult to identify in satellite images: (a) fluvial flooding, (b) shadows from valley walls, (c) cloud cover and (d) sea-ice and snow. Background image for all examples is a Sentinel-2 true colour image.

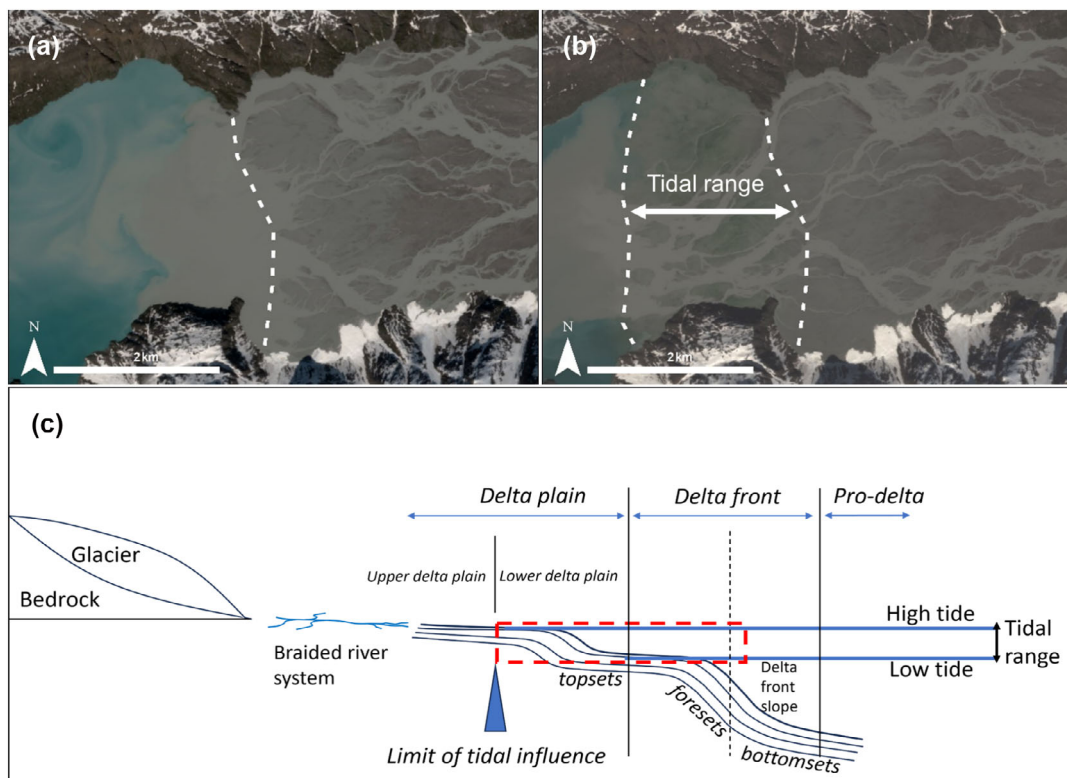


FIGURE 4 Example of the difference between (a) high and (b) low tides between two consecutive Sentinel-2 satellite images. (a) High tide (+0.71 m) on 17 June 2021 and (b) low tide (−0.75 m) on 21 June 2021. This modelled tidal range of 1.46 m over a distance of ~ 2 km is roughly consistent with the measured delta slope, which shallows from ~ 1.3 m/km near Sermeq Glacier to ~ 0.5 m/km at the delta front. (c) Schematic diagram illustrating the impact of fluctuating tidal cycle on the delta area. The red dashed box denotes the area over which sea level height variations influence the position of the delta shoreline from satellite imagery. No spatial or temporal scale is implied (vertical scale is exaggerated). Sermeq Glacier is approximately 65–70 km long, and the Sermilik Delta measured approximately 16 km in length on the 9 September 2022 at low tide.

2.4 | Tidal correction method

To enhance the precision of our delta area change observations, we implemented a tidal correction. This approach addresses the impact of sea level height variations caused by tides on the position of the satellite-derived delta shorelines, which are affected by the slope of the delta surface (Wicaksono et al., 2018). This correction method assumes that an observed horizontal shift in shoreline position mostly reflects tidal height variation rather than delta progradation. Thus, by removing the tidal signal, real changes in the delta area over time can be isolated (e.g., Figure 5c). The tidally corrected delta area (cA) was determined by finding the relationship between tidal height change (dh) and the corresponding observed delta area change (dA) and subtracting this from the raw delta area (A):

$$cA = A - (s * h + b) \quad (1)$$

Where s represents the slope of the linear relationship between dA and dh , h is the tide height for the corresponding A , and b is the

intercept. We make the assumption that the slope of the delta surface is constant and uniform.

Preliminary investigation into the influence of tides on the delta area revealed a consistent and statistically significant inverse relationship between dh and dA for all time periods tested (single month outside of the melt season, annual periods and multi-annual periods) (e.g., Figure 5a,b). This suggests that tidal sea surface height changes play a significant role in driving observed delta area changes, consistent with the observed several-kilometre tidal variation (mean modelled tidal range: 2.6 m) in shoreline position along the low-angled (~ 1.3 m/km) delta plain (Figure 4), compared to ~ 150 m year $^{-1}$ rate of delta progradation between the 1980s and 2010s (Bendixen et al., 2017). This dominance of the tidal signal allowed the correction to be calculated across whole years with sufficient data. For previous periods, with sparse data coverage, we used multi-annual periods: 1987–1999, 2000–2004, 2005–2009, 2010–2015 and 2016–2022.

Upon initial inspection of the raw delta area data, no significant changes in area were observed on an annual timescale (2016–2022) (e.g., Figure 5a). We suggest this is because tidal heights fluctuate

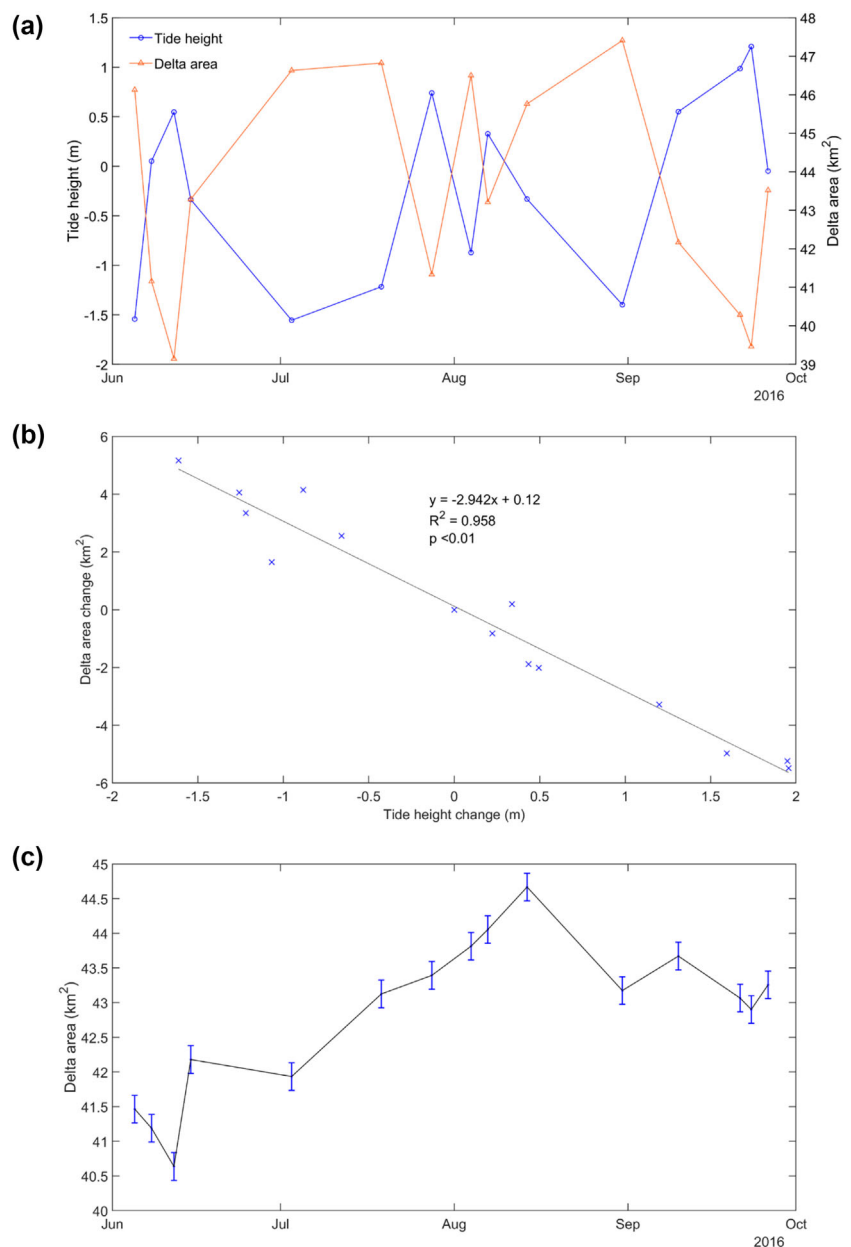


FIGURE 5 (a) Time series of tide height and delta area data for 2016. (b) Linear regression plot showing the relationship between tide height change and delta area change for 2016. (c) Tidally corrected delta area data for 2016 showing standard error bars.

annually and are higher in spring and autumn, resulting in apparent changes in dA that actually reflect variations in dh . By removing the tidal signal, we are able to extract the underlying trend in dA over sub-annual periods (Figure 5c), providing a more accurate signal of delta progradation on shorter timescales, and giving confidence that the modelled tidal data is producing realistic values.

2.5 | Tidal correction evaluation

Figure 6 shows the delta area data from 1987 to 2022, before and after the tidal signal was removed from the time series. A power law curve was used to model the observed data due to the nonlinear nature of the delta area changes over time. Prior to removing the tidal signal, the quality of fit is represented by an R^2 of 0.82. The application of the tidal correction improved the model's performance ($R^2 = 0.97$) and reduced the variability (Figure 7). Without the tidal correction, delta growth rate would be overestimated.

2.6 | Delta area change quantification

To quantify the change in dA between periods, the 5th and 95th percentile values of each year were used as metrics to represent, without outliers, the early season and late-season conditions, respectively. The 5th percentile data point represents the minimum observed delta area extent for a particular year, while the 95th percentile data point represents the maximum. The change in delta area extent is calculated as

$$dA = A_i - A_j \quad (2)$$

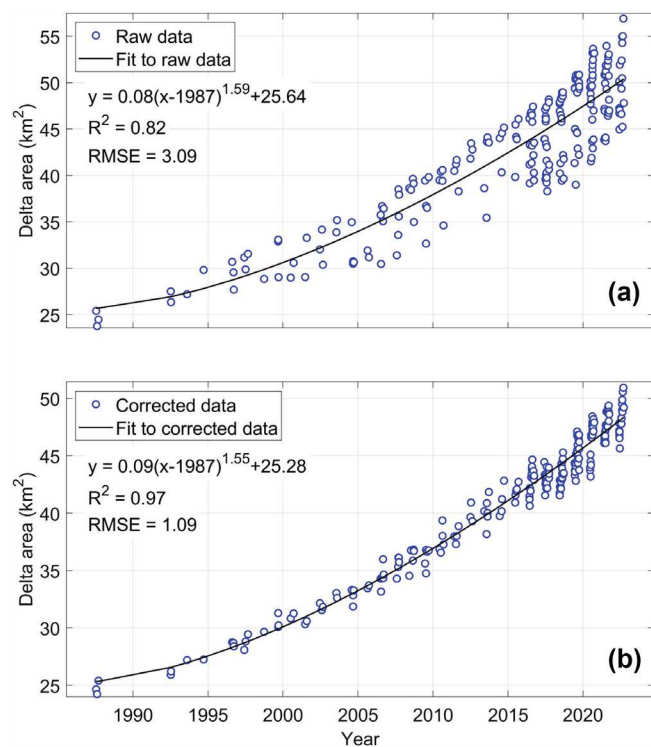


FIGURE 6 The effect of applying the tidal correction. (a) The raw delta area data before the tidal correction. (b) The delta area data after the tidal signal was removed.

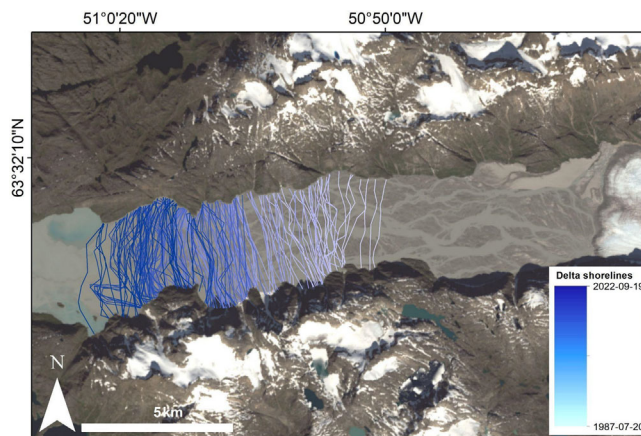


FIGURE 7 Map of delta front positions from 1987 to 2022. Background image is a Landsat 9 true colour image (taken on 13 August 2022). Light (earliest) to dark blue (latest) margin positions indicate the delta front position through time. Note the prominent advancing delta lobe located on the southern edge of the delta front in later years (e.g., 2020). The glacier terminus is stable throughout the study period.

where A_i (A_j) represent the 95th (5th) percentile value of the delta area for a specific year. This approach is then used to obtain the overall area changes. To determine the annual area change accounting for yearly variations, we use the 95th percentile value of each year as a representative measure of delta area change post-hydrological melt season, capturing late-season area fluctuations. This approach was chosen due to its ability to capture the upper range of data distribution, which is particularly informative when investigating interannual variations in delta area change.

2.7 | Subglacial discharge

To understand the relationship between catchment runoff and delta morphodynamics, modelled daily meltwater discharge data were obtained from Mankoff et al. (2020). Meltwater discharge was calculated using daily runoff estimates from the Regional Climate Model (RACMO) version 2.3p2 (Noël et al., 2019), routed subglacially to the catchment outlet. The dominant outlet and basin that contributed to the runoff entering the fjord were selected for the study area, and the melt-season (June–September) discharge total was calculated. To investigate the impact of episodic high discharge events on delta area change, we calculated the number of extreme discharge events using two methods. First, we used the Hampel identifier, typically used for outlier detection in time-series data (e.g., Sharifi et al., 2022), to isolate extreme discharge values by comparing each value with a running median and median absolute deviation. This approach allowed us to generate a relative metric, providing insight into the additional geomorphic power that extreme events might exert beyond the background discharge, indicating the potential for enhanced erosion and sediment transport during floods. Second, we calculated the 95th percentile of all daily discharge values to count the number of extreme events for each year, providing an absolute metric that serves as a proxy for the overall geomorphic power of the discharge.

2.8 | Tidal discharge

Once sediment reaches the intertidal zone, both fluvial and tidal processes control delta change (Fagherazzi & Overeem, 2007; Hoitink et al., 2017). The relative dominance of tidal and river processes was quantified by comparing fluvial and tidal discharge (e.g., Nienhuis et al., 2018); when tidal discharge is much greater than fluvial discharge, tidal processes dominate, and vice-versa. For Sermilik Delta, we calculated a mean tidal discharge of $373 \text{ m}^3 \text{ s}^{-1}$ based on the mean tidal range (2.6 m), fjord width (3.1 km) and delta slope (1.3 m/km) and the 6-h ebb tide.

2.9 | Ice velocity data

Ice flow velocities at the Sermeq Glacier were obtained using data from the NASA MEaSUREs ITS_LIVE programme (Gardner et al., 2018; Gardner et al., 2019), which contains annual ice velocity mosaics of the GrIS, generated from Landsat imagery covering the

period from 1985 to 2018 and gridded to 240 m (Gardner et al., 2018; Gardner et al., 2019). Median annual ice velocity was extracted from the average of all pixels in the glacier catchment that have data for all years (excluding 1987–1991 when there was very little velocity data due to insufficient satellite coverage), and average ice flow across the study period exceeds 50 m year^{-1} .

2.10 | Fjord width

Accommodation space is determined by fjord width and bathymetry. Fjord width was measured at each delta shoreline position. The fjord walls and a centreline were delineated, and then to ensure the measurements were representative, the fjord width was measured perpendicular to the main along-fjord axis at the point where the delta shoreline intersects the centreline. The median fjord width for each year was calculated to evaluate its impact on delta area change.

A key limitation of this study is the lack of bathymetry data to fully constrain the 3D geometry of Sermilik Fjord. For the same

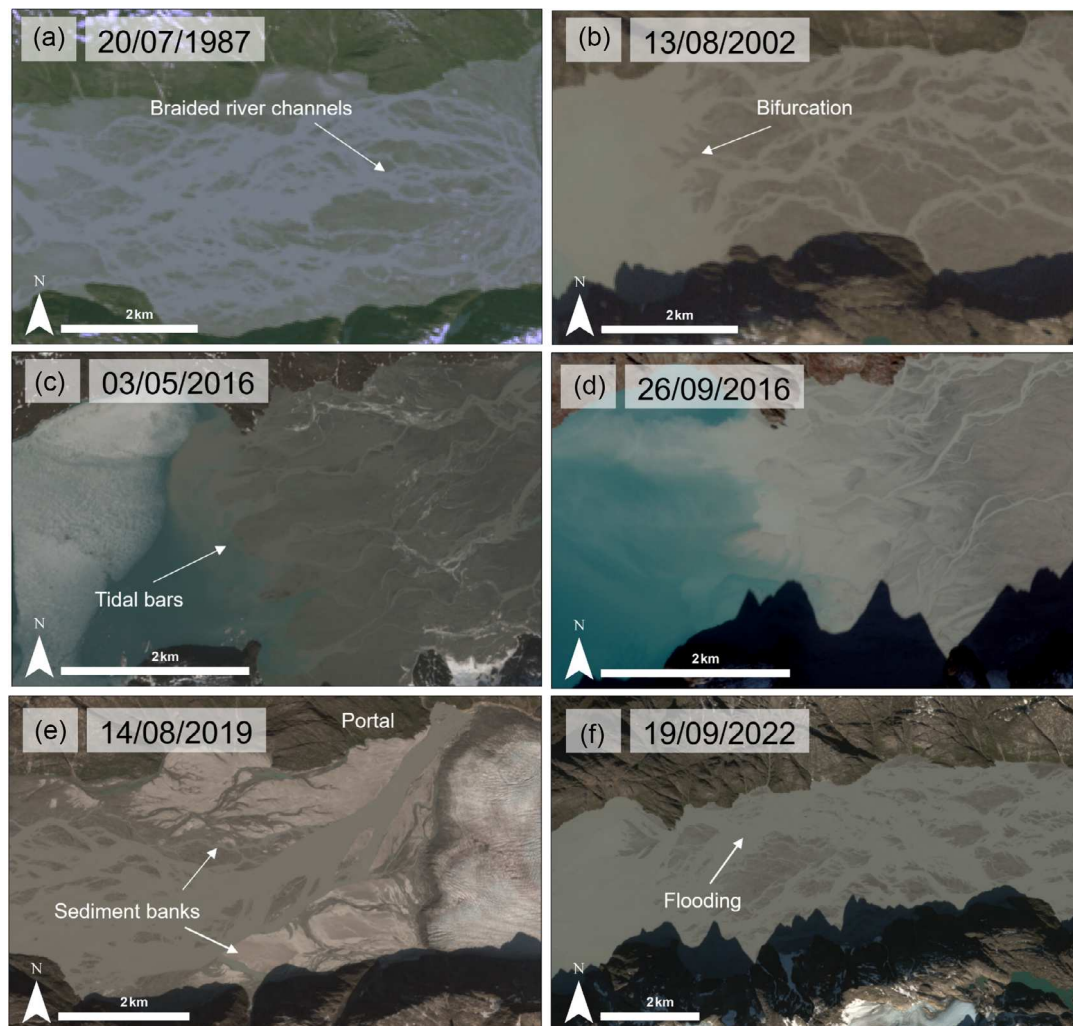


FIGURE 8 Examples of key geomorphological features of the Sermilik Delta system during its evolution. (a) Example of the typical braided river channels emanating from Sermilik glacier. (b) Distributary channel networks showing mouth-bar-induced river bifurcation. (c) Elongation of a tidally influenced mouth bar. (d) Tidal reworking along the delta fringe. (e) Example of sediment banks forming proximal to the subglacial portal, associated with temporary stabilisation following sediment aggradation. These banks become inundated during high flow. (f) Flooding of the delta during a large discharge event resulting in almost complete inundation of the delta plain. Background image (a) Landsat 5, (b) Landsat 7 and (c)–(f) Sentinel-2.

sediment flux, progradation would be slower when the fjord is deeper and faster when the fjord is shallower. While we cannot rule out the possibility of progradation rates being strongly controlled by variations in bathymetry, the consistent width and lack of tributaries of Sermilik Fjord (Figure 1) suggests it is less likely to exhibit large spatial variations in glacial erosion and thus bathymetry, potentially reducing this impact (Patton et al., 2016).

3 | RESULTS

3.1 | Geomorphological features of the delta system

Satellite imagery reveals ~10-km advancement of the delta in the down-fjord direction between 1987 and 2022, while the glacier terminus remained stable (Figure 7). The delta system is characterised by a braided river plain (Figure 8), which experiences frequent fluvial inundation during the melt season resulting in shifts in the braided channels (Figure 8a). Distinct seasonality of the delta system is observed, including freezing over of river channels during the winter and the presence of sea-ice in the fjord, typically between the months of October/November to May. River channels currently emerge from two dominant subglacial portals, located at the northern and southern ends of the glacier terminus, although the relative discharge from each has changed qualitatively through time. Sediment aggradation near the subglacial portals is indicated by bar growth, and the formation of sediment banks, which inundate occasionally but can be stable over successive years (Figure 8e). The distributary channel networks often increase in number at the delta front and exhibit mouth-bar-induced bifurcation, illustrating the influence of fluvial input into the delta system (Figure 8b) (Geleynse et al., 2011). Tides influence the morphology of the delta front through the formation of shore-perpendicular elongate tidal bars (Figure 8c) that form quasi-parallel to the tidal flow (Dalrymple & Choi, 2007). Tributary channels also become enlarged by tidal motion during times of low fluvial input and show less order of branching than when river flow dominates (Figure 8d) (Plink-Björklund, 2012).

3.2 | Evolution of the Sermilik Delta from 1987 to 2022

Between 1987 and 2022, significant progradation of the delta occurred ($R^2 = 0.97$, $p < 0.01$). The delta area increased in the down-fjord direction by approximately 26.37 km², from 24.27 km² in 1987 to 50.64 km² in 2022 (108% area increase) at an average rate of 0.78 km² year⁻¹. The annual progradation rate reveals a superlinear trend (Figure 9a) represented by a power law regression curve ($R^2 = 0.99$):

$$y = 0.10(x - 1987)^{1.54} + 25.25 \quad (3)$$

We applied Bayesian change-point detection (BEAST; Zhao et al., 2019) to determine statistically significant shifts in the time series. A statistically significant shift in delta growth was identified in

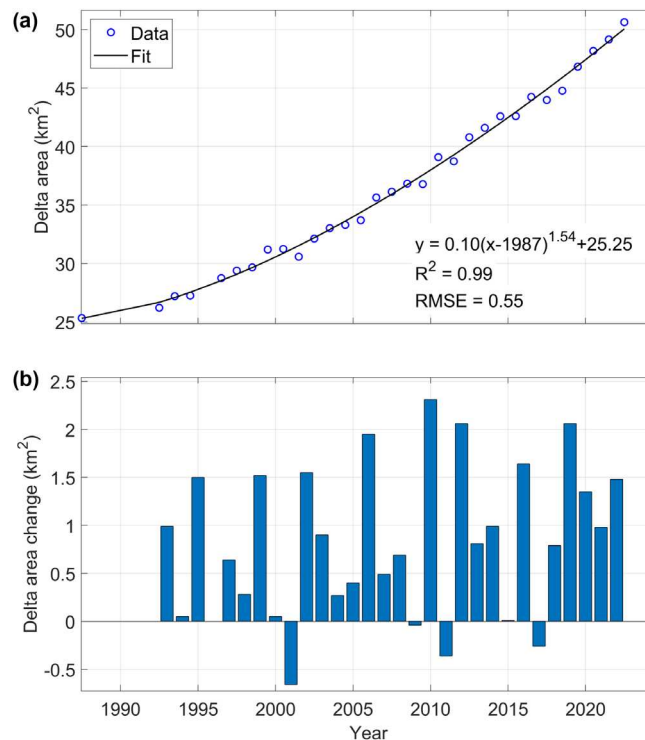


FIGURE 9 (a) Annual area change of the Sermilik Delta from 1987 to 2022 (95th percentile with power law curve fit). (b) Interannual delta area change (95th percentile difference from 1 year to the next). The annual 95th percentile value gives a representative value of the magnitude of change in the delta area following the hydrological melt season and to capture the late-season area.

1994. From 1987 to 1994, delta area increased by 1.92 km² at a rate of 0.27 km² year⁻¹. In contrast, from 1994 to 2022, delta growth was much more rapid, increasing by 23.4 km² overall at a rate of 0.84 km² year⁻¹. During the final 5 years of the study period (2017–2022), the delta grew by 8.55 km², corresponding to an increased progradation rate of 1.35 km² year⁻¹, which is 73% greater than the overall average.

On an interannual scale, the magnitude of delta area change varies considerably between successive years and is punctuated by years of significant growth (Figure 9b). Substantial increases in the delta area occurred in 2006, 2010, 2012 and 2019. Conversely, 2001, 2011 and 2017 are marked by decreases in delta area. Analysing short-term changes in delta area, between every data point, was only possible for the years 2016–2022 when the temporal resolution of the data was significantly improved by the availability of Sentinel-2 satellite imagery (Figures 6, 10). These data display an increasing trend throughout the summer melt seasons when river discharge is typically greater than tidal discharge, but with variability between individual data points. In the period 2016–2022, all years except for 2017 ($R^2 = 0.18$, $p = 0.07$) exhibit significant seasonal increases in delta area. Large magnitude melt events are often associated with periods of accelerated delta growth, for example, in July 2018 (Figure 10c) and August 2020 (Figure 10e). Conversely, four of the six October to May periods were characterised by a decrease in delta area, and periods of slower growth or recession often occur during low flow period when tidal discharge exceeds river discharge (Figure 10).

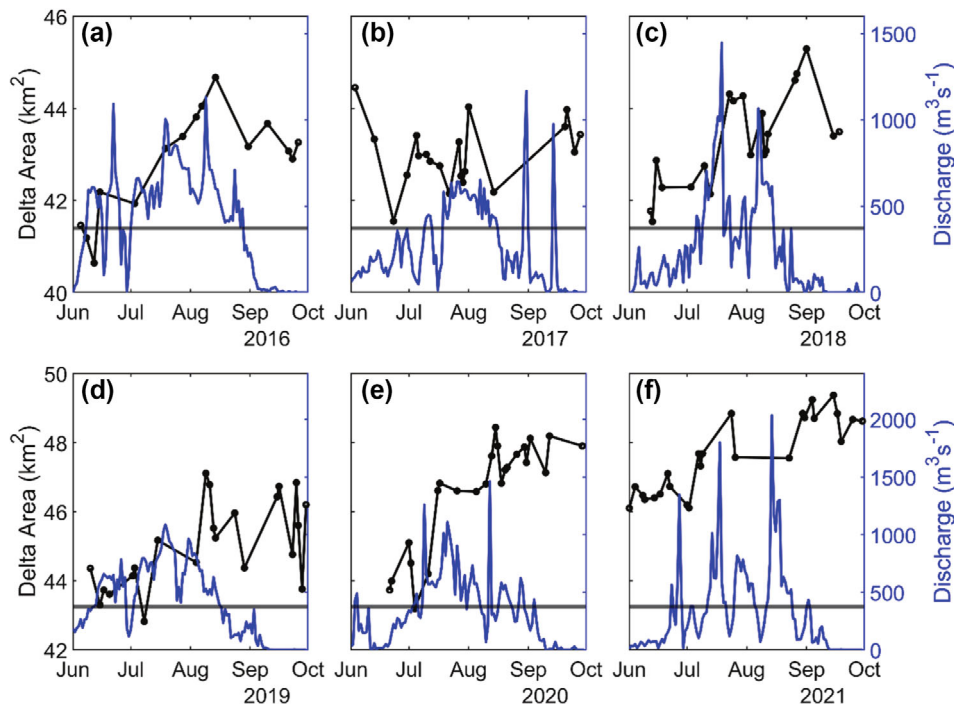
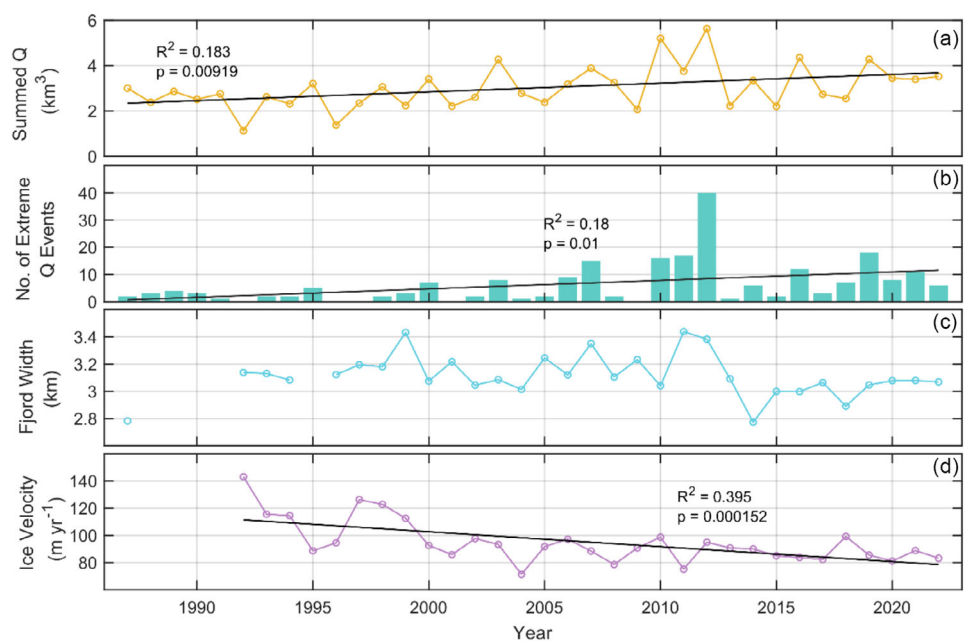


FIGURE 10 Time series of delta area change (blue line) and discharge (black line, from Mankoff et al., 2020) between June and October 2016–2021. The black horizontal line is the tidal discharge (see Methods). When river discharge is less than the tidal discharge, flow is likely to be tidally dominated. When river discharge exceeds the tidal discharge, fluvial processes will dominate.

FIGURE 11 Interannual trends of environmental controls at Sermilik Delta between 1987 and 2022.

(a) Summed discharge (Q). (b) Number of extreme discharge events (95th percentile). (c) Fjord width. (d) Median ice velocity. Summed discharge and extreme discharge events display significant (<0.05) positive trends through time, while median ice velocity exhibits a significant (<0.01) negative trend.



3.3 | Controls governing delta area change

There is a significant positive trend in summed discharge ($p < 0.01$) from Sermilik Glacier, and the number of extreme discharge events ($p < 0.05$) between 1987 and 2022 (Figure 11). Summed discharge (i.e., total meltwater volume) has increased at a rate of 0.038 km^3 per year (17% increase over the 35-year study period), with the three greatest runoff years in 2010, 2012 and 2016. Bayesian change-point detection (Zhao et al., 2019) identified a statistically significant shift in summed discharge in 2010. In contrast, ice velocity displays a significant ($p < 0.01$) negative trend across the study period, decreasing

from a median velocity of 114 m year^{-1} between 1994 and 1998 to 85 m year^{-1} between 2018 and 2022 (25% decrease over the 30-year period). The section of the fjord traversed by the delta front during the study period has a mean width of $3.1 \pm 0.15 \text{ km}$ and displays no significant trend in width along the fjord.

Linear regression analysis demonstrates a significant relationship between key melt-season discharge variables and annual delta change between 1992 and 2022 (1987–1991 omitted due to lack of data) (Figure 12a,c,e). The summed discharge shows a significant positive relationship ($p < 0.05$). The adjusted- R^2 value is relatively weak (0.29) over the entire time period (Figure 12a) and not significant from 1992

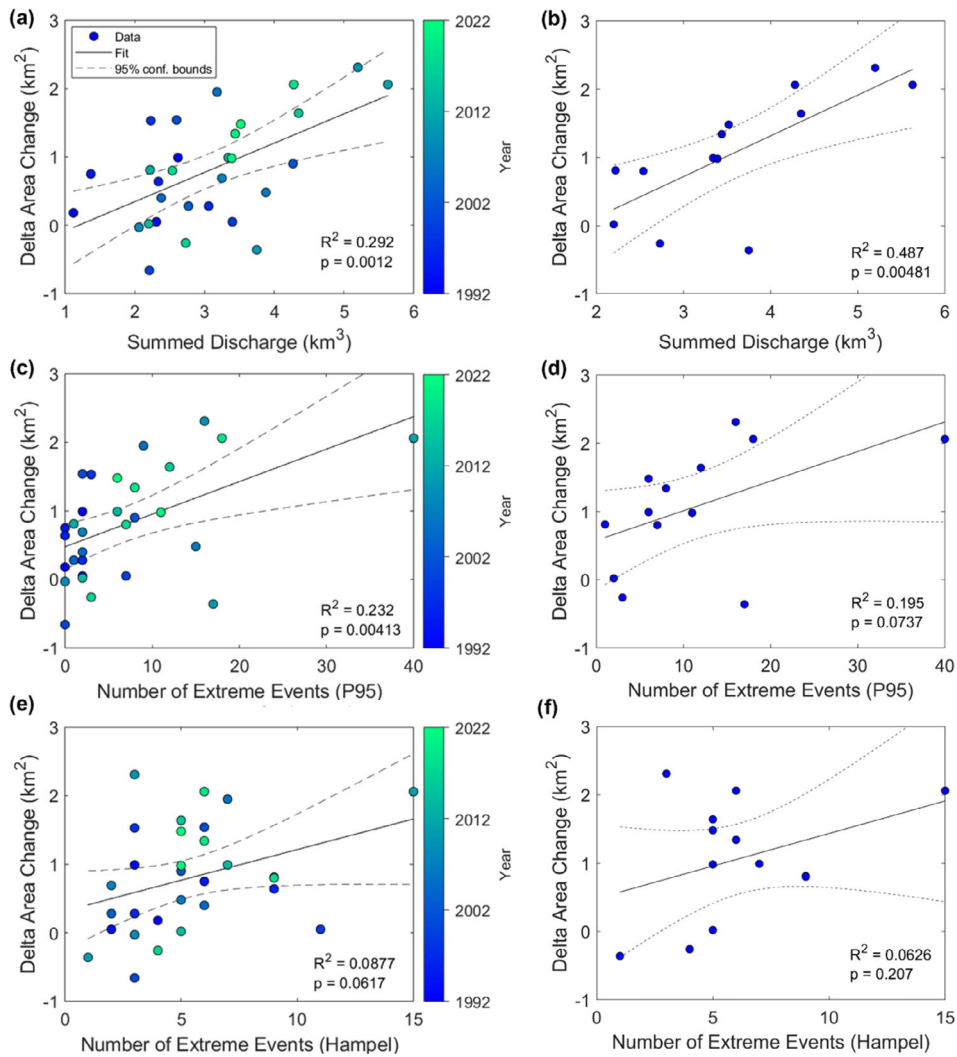


FIGURE 12 Linear regression of delta area change and melt-season discharge variables from 1992 to 2022 (a,c,e) and 2010 to 2022 (b,e,f). 1987–1991 was omitted due to lack of data. (a–b) Summed discharge. (c–d) Number of extreme discharge events per melt season, based on the 95th percentile of the daily discharge values (P95). (e–f) Number of extreme discharge events per melt season based on a Hampel identifier. Note that in (b) and (d) the large outlier is from 2011, which immediately followed a high melt year (2010).

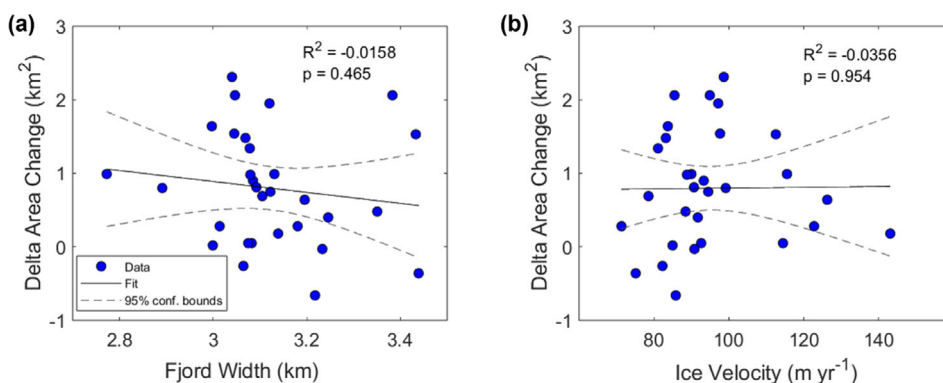


FIGURE 13 Linear regression of delta area change and environmental variables from 1992 to 2022. (a) Fjord width. (b) Ice velocity. The relationships for 2010 to 2022 were also not significant and so are not shown here.

to 2010 but shows a strong correlation (0.49) over the last 12-years of the study period (2010–2022) (Figure 12b). Noticeably, prior to 2010 there is considerably higher scatter in delta area change for similar summed discharges, particularly at lower values (Figure 12a).

Using the 95th percentile to represent the change in number of ‘absolute’ extreme discharge events per melt season reveals a significant but weak positive relationship with delta area change ($p < 0.05$,

adjusted- R^2 of 0.23) across the whole study period, and no significant correlation over the last 12 years (Figure 12c–d). The Hampel identifier, which provides a relative measure of extreme discharge events, shows no significant relationship with delta area for either time period (Figure 12e–f). Fjord width and ice velocity exhibit no significant relationship with delta area change on annual timescales, both over the whole time period and between 2010 and 2022 (Figure 13).

4 | DISCUSSION

This study provides the first annual resolution mapping and quantification of shoreline change for the Sermilik Delta, Greenland. Between 1987 and 2022, the delta more than doubled in area, and prograded at an accelerating rate, represented by a power-law relationship (Figure 9a). Superlinear delta growth indicates a substantial increase in the amount of sediment transport and connectivity within the Sermilik Glacier-Delta-Fjord geomorphic system.

Bendixen et al. (2017) reported progradation of Sermilik Delta at a rate of $0.47 \text{ km}^2 \text{ year}^{-1}$ for the period 1980–2010. This study derived a slightly faster progradation rate of $0.49 \text{ km}^2 \text{ year}^{-1}$ between 1987 and 2010, representing a 4.3% difference, likely due to slightly different time periods and the higher temporal resolution mapping conducted in this study, made possible by the use of a tidal correction. However, overall, the two approaches are comparable. For the period 1940–1980, the delta prograded at a significantly slower rate of $0.16 \text{ km}^2 \text{ year}^{-1}$ (Bendixen et al., 2017). Between 2017 and 2022, the progradation rate of the delta was $1.35 \text{ km}^2 \text{ year}^{-1}$, reflecting a 744% increase compared to the 40-year period from 1940 to 1980.

4.1 | Delta area change and meltwater runoff forcing

Our results demonstrate that changes in delta area and therefore sediment input and transport are significantly influenced by meltwater runoff (Figure 12). This association between delta area change and meltwater runoff is apparent when examining summed discharge, as well as for extreme discharge events (95th percentile).

Meltwater runoff has been identified as a dominant mechanism in controlling rates of sediment transfer in glacial and proglacial environments (e.g., Antoniazza & Lane, 2021; Beaud et al., 2016; Comiti et al., 2019; Cowton et al., 2012; Delaney & Adhikari, 2020; Herman et al., 2021; Swift et al., 2005). The positive correlation between delta area change and meltwater discharge suggests that increased meltwater production on the surface of the GrIS, linked to rising temperatures and negative mass balance (e.g., Beckmann & Winkelmann, 2023), reaches the ice bed and has a direct impact on sediment transport (e.g., Chu et al., 2012) and proglacial foreland dynamics (Bendixen et al., 2017; Hasholt et al., 2018; Overeem et al., 2017; Savi et al., 2023). Increased meltwater input to the subglacial environment leads to enhanced subglacial sediment transport, with the transport capacity increasing superlinearly with discharge (e.g., Alley et al., 1997; Swift et al., 2005). This relationship is consistent with our findings, which reveal accelerating delta growth (Figure 9a) in response to a linear increase in meltwater discharge (Figure 11a,b).

4.2 | Impact of episodic extreme discharge events

Intensified glacier melting not only increases summer discharge but also amplifies discharge variability and the frequency and magnitude of extreme events (Lane & Nienow, 2019; Slater et al., 2021; Zhang et al., 2023). Our results show a significant but weak positive

relationship between delta growth and the increasing frequency of extreme (95th percentile) subglacial discharge events between 1992 and 2022 (Figures 12c), consistent with the high erosion and sediment transport capabilities of large floods (Alley et al., 1997), and observations of sediment fluxes dominated by high-magnitude episodic events in glaciated basins (e.g., Carrivick & Tweed, 2021; Dunning et al., 2013; Hasholt et al., 2008; Livingstone et al., 2019). This includes the ability of extreme discharge events to erode and mobilise new subglacial sediment and remobilise sediment downstream in the proglacial zone. In contrast, the Hampel identifier produces no significant temporal trend in the frequency of 'relative' (i.e., more than three times the median absolute deviation from the 30-day median) extreme discharge events and no correlation with delta area change (Figure 12e–f). We interpret this to indicate that the correlation between delta area change and extreme discharge events at Sermilik is not dependent on the relative increase in discharge compared to the background signal, but scales more closely to absolute discharge variability.

Greenland experienced several extreme melt periods, with 2010 (Tedesco et al., 2011), 2012 (Nghiem et al., 2012) and 2019 (Tedesco & Fettweis, 2020) corresponding to the years with the highest number of extreme events (95th percentile) and the largest expansion of Sermilik Delta (Figure 9b). These melt events are linked to a strong negative North Atlantic Oscillation (NAO) index, resulting in persistent anticyclonic pressure over Greenland—commonly referred to as blocking-events (Beckmann & Winkelmann, 2023; Bevis et al., 2019; Hofer et al., 2017; Tedesco & Fettweis, 2020).

4.3 | Proglacial foreland expansion and sediment connectivity

The influence of runoff on delta area change has strengthened in recent years. While there is no significant correlation between delta area change and summed discharge between 1992 and 2010 (p -value >0.05), there is a statistically significant (p -value <0.01) and strong (adjusted- $R^2 > 0.4$) relationship after 2010. We suggest the stronger relationship reflects enhanced sediment connectivity between stream channels and sediment sources due to the frequent migration of braided channels and flooding of the proglacial zone, accessing, reworking and remobilising proglacial sediment (e.g., Lane et al., 2017), driven by increased melt (average and extreme events) and expansion of the delta plain itself. This is analogous to studies that have linked glacier retreat and paraglacial activity to enhanced sediment yields (e.g., Ballantyne, 2002; Lane et al., 2017), although here expansion of the proglacial area has occurred due to delta growth rather than glacier retreat.

When the delta plain was smaller earlier in the study period, we suggest subglacial processes would have been relatively more important in controlling sediment production and transport to the delta front. However, the relationship between subglacial hydrology and sediment flux is complex (Cowton et al., 2012; Hudson et al., 2014). This is because each summer the subglacial drainage system typically forms discrete channels—evidenced by the subglacial portals discharging water onto the foreland (Figure 8)—limiting the portion of the bed where meltwater can erode and transport sediment (Cowton et al., 2012; Hasholt et al., 2018). Thus, annual proglacial sediment

flux depends not only on total meltwater discharge but also on the availability of sediment. More sediment can be accessed by the opening of new subglacial channels and the migration, expansion or overpressurisation of existing subglacial channels (Bogen, 2008; Delaney & Adhikari, 2020; Delaney et al., 2018; Lewington et al., 2020). Sediment flux will not increase with meltwater discharge if sediment supply is limited (Hasholt et al., 2018). For example, although 2011 was one of the highest discharge years (Figure 11a,b), it was characterised by a reduction in delta area (Figure 9b), possibly caused by sediment exhaustion from the flushing of sediment during the exceptionally high melt year directly preceding it in addition to tidal and wave erosion. In contrast, the 3 years with greatest delta growth are all after 2010 and follow relatively low discharge years (Figure 11). Thus, during the earlier expansion of the delta, we suggest annual variability in delta area change is more strongly associated with shifts in the location of subglacial channels and changing access of meltwater to fresh basal sediment sources (e.g., Bogen & Bønsnes, 2003; Cowton et al., 2012; Delaney & Adhikari, 2020), resulting in a non-significant overall correlation with discharge ($p > 0.05$, 1992–2010).

Expansion of the proglacial area, which doubled in size between 1987 and 2022, would have increased access to unconsolidated sediment (e.g. Leggat et al., 2015). During years with high meltwater discharge or during high-magnitude floods (both of which are increasing through time, Figure 11a–c), the proglacial foreland is inundated, and channels migrate laterally (Figure 8), facilitating large-scale sediment remobilisation (Carrivick & Tweed, 2021; Comiti et al., 2019; Hasholt et al., 2018; Lane et al., 2017; Mancini et al., 2023). In particular, large floods are capable of mobilising coarse sediments across the whole delta plain, strengthening the lateral connectivity (e.g., Lane et al., 2017; Savi et al., 2023). This leads to the downstream transfer of sediment to the delta front that is at least partially captured by the annual signal of delta area change.

There was no direct correlation between discharge and delta progradation at sub-annual timescales between 2016 and 2022. This likely reflects lags in the system of transporting coarser sediment across the delta plain to the ocean (e.g., Mancini et al., 2023; Mao et al., 2017). Specifically, sediment build-up near the subglacial portals and the stabilisation of sediment banks (e.g., Figure 8e) over successive melt seasons indicates that coarse sediment load is deposited in the ice-proximal area and can become temporarily disconnected from the main proglacial sediment system (e.g., Comiti et al., 2019; Savi et al., 2023). There will also be a delay between when sediment is flushed out from the subglacial environment, deposited in the ice-proximal proglacial area, transported onto the delta outwash plain, and when the resulting progradation signal is evident at the delta shoreline. This is consistent with studies that suggest that the timescale of bedload transport is much longer than that of discharge (Mancini et al., 2023; Mao et al., 2017). Similar to the paraglacial model (Church & Ryder, 1972), we might eventually expect sediment fluxes to the delta front to decline even with increasing discharge due to exhaustion of sediment stores under the glacier (de Winter et al., 2012) and negative feedbacks such as storage in lake basins exposed by ice recession (How et al., 2021), and in the river plain, due to the increased transport distance for sediment to reach the ocean.

4.4 | Impact of other environmental variables on delta area change

Ice velocity and fjord width exhibit no significant correlation with delta growth (Figure 13). The lack of correlation with ice velocity contrasts with Overeem et al. (2017), who suggest that although runoff explains some of the variance in suspended sediment concentration around the GrIS, it is more strongly controlled by ice dynamics. Indeed, delta growth has accelerated at Sermilik despite a long-term slowdown in median ice velocity (Figure 11e). We suggest the two results reflect different spatial- and temporal-scales of study. Overeem et al. (2017) calculated an erosional potential for each catchment around the GrIS at a snapshot in time, demonstrating that larger, faster flowing glaciers tend to generate more sediment. However, within individual catchments, unless the system becomes supply-limited (e.g., Riihimaki et al., 2005), short-term (annual) fluctuations are likely to be controlled by the transport of stored sediment to the terminus (i.e., sediment connectivity and transport capacity) rather than the erosion rate. These subglacial sediment stores can build up and be released over multi-millennial timescales (de Winter et al., 2012). The high erosional potential of Sermilik Glacier (Overeem et al., 2017), and large and expanding proglacial store of sediment, suggests it is not supply-limited, and therefore that delta growth results from variations in runoff impacting the transport capacity and connectivity to stored sediment, rather than bedrock erosion.

We expect fjord width to impact delta growth by changing the cross-sectional area that needs to be filled by sediment for delta expansion, that is, a narrow fjord should lead to faster expansion than a wider fjord for a given sediment flux. The lack of correlation between delta progradation rate and fjord width might reflect the relatively consistent width of Sermilik fjord, limiting its overall influence compared to sediment flux, and/or poor constraints on fjord bathymetry and thus the true 3D accommodation space. In particular, we cannot fully rule out the possibility that accelerating delta growth is a response to bathymetric shallowing. However, we suggest this is unlikely primarily based on the lack of any correlation with fjord width (Figure 13a). This is because width is a key component of the volume calculation and overdeepenings typically exhibit a positive width-depth relationship (see Patton et al., 2016), so we expect width to be a reasonable proxy for accommodation space.

4.5 | Tidal impact on delta morphology

A significant finding of this research is the importance of incorporating tidal sea surface height variations in calculating delta area change. Satellite imagery demonstrates that the tidal regime within the Sermilik Fjord is a fundamental feature of the delta system (Figure 8c,d). We demonstrate that the fluctuating tidal cycle dominates delta shoreline variations on a sub-annual timescale, obscuring any signal from changes in meltwater runoff (Figure 5). The tidal correction method used in this study increases the overall reliability and accuracy of the delta area change results (Figure 6). This improves on methods that have relied on identifying the high-waterline (Bendixen et al., 2017), which is likely to introduce error due to the subjective approach and variations in high tide magnitudes. Our correction has

enabled more precise and consistent measurements of delta area, which is crucial for comparing changes at annual timescales.

In general, during the melt season the delta is fluvially dominated (i.e., river discharge >>tidal discharge), consistent with delta growth from the transport of large volumes of sediment by Sermeq River into the fjord. However, during lower flows (largely but not exclusively outside of the melt season), river discharge drops below mean tidal discharge (Figure 10), and tides become the dominant geomorphic process. The morphological impact of tidal processes is evidenced by the form of elongated bars at the delta front (Dalrymple & Choi, 2007) (Figure 8c) and widening of channels by tidal motion (Nienhuis et al., 2018) (Figure 8d). Given that delta growth is slower or can recede outside of the melt season and during low flows (Figure 10), we suggest that tidal erosion processes control delta morphology during these periods.

5 | CONCLUSION

This study investigated the annual morphodynamic evolution of the Sermilik Delta, on the southwest coast of Greenland (1987–2022) from satellite-derived shorelines and modelled tides. We highlight the significant role of tides on the morphodynamics of proglacial deltas during periods of low ice sheet runoff and the complexity in extracting the impact of runoff variations on delta area change. To address the latter effect of tidal water height variations on mapping, we apply a tidal correction, which involves removing the tidal signal from the delta shoreline dataset to minimise its impact on the delta area change time series, improving the overall reliability and accuracy.

Our results indicate that the Sermilik Delta has expanded ~26 km² from 1987 to 2022 (0.78 km² year⁻¹), a 108% increase in overall delta area. Delta growth has been accelerating, with increasing runoff the primary driver of enhanced sediment delivery and delta progradation, rather than ice velocity, which decreases during the study period. Periods of significant and pronounced area change often correspond to high meltwater runoff years, highlighting the sensitivity of this system to recent glacier mass loss. With the Arctic warming faster than the rest of the world (Dai et al., 2019) and surface melt and runoff expected to dominate GRIS mass loss and retreat over the next century (Fürst et al., 2015), increasing sediment yields are expected at Sermilik and other glacier catchments that have access to stores of subglacial sediment (i.e., that are not supply-limited). We demonstrate that over decadal timescales increased sediment fluxes can occur despite slowdown in ice flow, likely due to lags in sediment storage and release. This high-resolution (annual) study therefore supports previous coarser (decadal) temporal resolution work highlighting the widespread progradation of deltas and correlation with glacier mass loss in southwest Greenland (Bendixen et al., 2017).

The coupling between runoff and delta change has strengthened through time, which we interpret to indicate enhanced sediment connectivity due to (i) an increasing supply of sediment from the expanding proglacial foreland, reducing the dependence on the subglacial drainage system eroding and accessing new sediment sources; and (ii) greater sediment transport capacity from increasing discharge and extreme discharge events. This implies a transition from a supply-limited to a transport-limited system with accelerating sediment yields

at the delta front disconnected from current glacier erosion rates, which are likely reducing in response to glacier slowdown.

ACKNOWLEDGEMENTS

Dr. Brice Noël (Utrecht University) provided access to the RACMO dataset.

CONFLICT OF INTEREST STATEMENT

We report no conflicts of interest.

DATA AVAILABILITY STATEMENT

Shapefiles of mapped shorelines are available at <https://doi.org/10.15131/shef.data.29209556>. The NASA MEaSUREs ITS_LIVE ice velocity product (Gardner et al., 2019) was generated using auto-RIFT (Gardner et al., 2018) and accessed via <https://nsidc.org/apps/itslive/>. Satellite images used for figures were downloaded from USGS EarthExplorer (www.earthexplorer.usgs.gov) and ESA Copernicus (<https://scihub.copernicus.eu/>). The Gr1kmTM tidal model data were developed using the Regional Ocean Modelling System (ROMS) and accessed via the Arctic Data Centre (<https://arcticdata.io/>).

ORCID

Stephen J. Livingstone  <https://orcid.org/0000-0002-7240-5037>

REFERENCES

- Alley, R.B. (1992) How can low-pressure channels and deforming tills coexist subglacially? *Journal of Glaciology*, 38(128), 200–207. Available from: <https://doi.org/10.3189/S0022143000009734>
- Alley, R.B., Cuffey, K.M., Evenson, E.B., Strasser, J.C., Lawson, D.E. & Larson, G.J. (1997) How glaciers entrain and transport basal sediment: physical constraints. *Quaternary Science Reviews*, 16(9), 1017–1038.
- Alley, R.B., Cuffey, K.M. & Zoet, L.K. (2019) Glacial erosion: status and outlook. *Annals of Glaciology*, 60(80), 1–13. Available from: <https://doi.org/10.1017/aog.2019.38>
- Antoniazza, G. & Lane, S.N. (2021) Sediment yield over glacial cycles: a conceptual model. *Progress in Physical Geography: Earth and Environment*, 45(6), 842–865.
- Aschwanden, A., Fahnestock, M.A., Truffer, M., Brinkerhoff, D.J., Hock, R., Khroulev, C., et al. (2019) Contribution of the Greenland ice sheet to sea level over the next millennium. *Science Advances*, 5(6), eaav9396. Available from: <https://doi.org/10.1126/sciadv.aav9396>
- Ballantyne, C.K. (2002) Paraglacial geomorphology. *Quaternary Science Reviews*, 21(18–19), 1935–2017.
- Beaud, F., Flowers, G.E. & Venditti, J.G. (2016) Efficacy of bedrock erosion by subglacial water flow. *Earth Surface Dynamics*, 4(1), 125–145.
- Beckmann, J. & Winkelmann, R. (2023) Effects of extreme melt events on ice flow and sea level rise of the Greenland ice sheet. *The Cryosphere*, 17(7), 3083–3099. Available from: <https://doi.org/10.5194/tc-17-3083-2023>
- Bendixen, M. & Kroon, A. (2017) Conceptualizing delta forms and processes in Arctic coastal environments. *Earth Surface Processes and Landforms*, 42(8), 1227–1237. Available from: <https://doi.org/10.1002/esp.4097>
- Bendixen, M., Lønsmann Iversen, L., Anker Bjørk, A., Elberling, B., Westergaard-Nielsen, A., Overeem, I., et al. (2017) Delta progradation in Greenland driven by increasing glacial mass loss. *Nature*, 550(7674), 101–104.
- Bendixen, M., Nielsen, R.L., Plesner, J.L. & Minor, K. (2022) Opportunistic climate adaptation and public support for sand extraction in Greenland. *Nature Sustainability*, 5(11), 991–999.
- Bendixen, M., Overeem, I., Rosing, M.T., Bjørk, A.A., Kjær, K.H., Kroon, A., et al. (2019) Promises and perils of sand exploitation in Greenland.

- Nature Sustainability*, 2(2), 98–104. Available from: <https://doi.org/10.1038/s41893-018-0218-6>
- Bevis, M., Harig, C., Khan, S.A., Brown, A., Simons, F.J., Willis, M., et al. (2019) Accelerating changes in ice mass within Greenland, and the ice sheet's sensitivity to atmospheric forcing. *Proceedings of the National Academy of Sciences*, 116(6), 1934–1939.
- Boak, E.H. & Turner, I.L. (2005) Shoreline definition and detection: a review. *Journal of Coastal Research*, 21(4), 688–703.
- Bogen, J. (2008) The impact of climate change on glacial sediment delivery to rivers. *IAHS Publication*, 325, 432.
- Bogen, J. & Bønsnes, T.E. (2003) Erosion and sediment transport in high Arctic rivers, Svalbard. *Polar Research*, 22(2), 175–189. Available from: <https://doi.org/10.3402/polar.v22i2.6454>
- Carrivick, J.L. & Heckmann, T. (2017) Short-term geomorphological evolution of proglacial systems. *Geomorphology*, 287, 3–28.
- Carrivick, J.L. & Tweed, F.S. (2021) Deglaciation controls on sediment yield: towards capturing spatio-temporal variability. *Earth-Science Reviews*, 221, 103809. Available from: <https://doi.org/10.1016/j.earscirev.2021.103809>
- Chu, V.W., Smith, L.C., Rennermalm, A.K., Forster, R.R. & Box, J.E. (2012) Hydrologic controls on coastal suspended sediment plumes around the Greenland ice sheet. *The Cryosphere*, 6(1), 1–19. Available from: <https://doi.org/10.5194/tc-6-1-2012>
- Church, M. & Ryder, J.M. (1972) Paraglacial sedimentation: a consideration of fluvial processes conditioned by glaciation. *Geological Society of America Bulletin*, 83(10), 3059–3072. Available from: [https://doi.org/10.1130/0016-7606\(1972\)83\[3059:PSACOF\]2.0.CO;2](https://doi.org/10.1130/0016-7606(1972)83[3059:PSACOF]2.0.CO;2)
- Comiti, F., Mao, L., Penna, D., Dell'Agnese, A., Engel, M., Rathburn, S., et al. (2019) Glacier melt runoff controls bedload transport in Alpine catchments. *Earth and Planetary Science Letters*, 520, 77–86.
- Cook, S.J., Swift, D.A., Kirkbride, M.P., Knight, P.G. & Waller, R.I. (2020) The empirical basis for modelling glacial erosion rates. *Nature Communications*, 11(1), 1–7.
- Cowton, T., Nienow, P., Bartholomew, I., Sole, A. & Mair, D. (2012) Rapid erosion beneath the Greenland ice sheet. *Geology*, 40(4), 343–346.
- Dai, A., Luo, D., Song, M. & Liu, J. (2019) Arctic amplification is caused by sea-ice loss under increasing CO₂. *Nature Communications*, 10(1), 121. Available from: <https://doi.org/10.1038/s41467-018-07954-9>
- Dalrymple, R.W. & Choi, K. (2007) Morphologic and facies trends through the fluvial–marine transition in tide-dominated depositional systems: a schematic framework for environmental and sequence-stratigraphic interpretation. *Earth-Science Reviews*, 81(3–4), 135–174.
- de Winter, I.L., Storms, J.E. & Overeem, I. (2012) Numerical modeling of glacial sediment production and transport during deglaciation. *Geomorphology*, 167, 102–114.
- Delaney, I. & Adhikari, S. (2020) Increased subglacial sediment discharge in a warming climate: consideration of ice dynamics, glacial erosion, and fluvial sediment transport. *Geophysical Research Letters*, 47(7), e2019GL085672. Available from: <https://doi.org/10.1029/2019GL085672>
- Delaney, I., Bauder, A., Huss, M. & Weidmann, Y. (2018) Proglacial erosion rates and processes in a glacierized catchment in the Swiss Alps. *Earth Surface Processes and Landforms*, 43(4), 765–778.
- Doyle, S.H., Hubbard, A., Van De Wal, R.S., Box, J.E., Van As, D., Scharer, K., et al. (2015) Amplified melt and flow of the Greenland ice sheet driven by late-summer cyclonic rainfall. *Nature Geoscience*, 8(8), 647–653.
- Dunning, S.A., Large, A.R., Russell, A.J., Roberts, M.J., Duller, R., Woodward, J., et al. (2013) The role of multiple glacier outburst floods in proglacial landscape evolution: the 2010 Eyjafjallajökull eruption, Iceland. *Geology*, 41(10), 1123–1126. Available from: <https://doi.org/10.1130/G34665.1>
- Erofeeva, S., Padman, L. & Howard, S. L. (2020) Tide Model Driver TMD version 2.5, Toolbox for Matlab. GitHub. Retrieved 15 June 2023. https://www.github.com/EarthAndSpaceResearch/TMD_Matlab_Toolbox_v2.5
- Fagherazzi, S. & Overeem, I. (2007) Models of deltaic and inner continental shelf landform evolution. *Annual Review of Earth and Planetary Sciences*, 35(1), 685–715. Available from: <https://doi.org/10.1146/annurev.earth.35.031306.140128>
- Fürst, J.J., Goelzer, H. & Huybrechts, P. (2015) Ice-dynamic projections of the Greenland ice sheet in response to atmospheric and oceanic warming. *The Cryosphere*, 9(3), 1039–1062.
- Gardner, A.S., Fahnestock, M.A. & Scambos, T.A. (2019) [18 September 2023]: ITS_LIVE regional glacier and ice sheet surface velocities: Version 1. Data archived at National Snow and Ice Data Center; <https://doi.org/10.5067/6II6VW8LLWJ7>
- Gardner, A.S., Moholdt, G., Scambos, T., Fahnestock, M., Ligtenberg, S., Van Den Broeke, M., et al. (2018) Increased West Antarctic and unchanged East Antarctic ice discharge over the last 7 years. *The Cryosphere*, 12(2), 521–547. Available from: <https://doi.org/10.5194/tc-12-521-2018>
- Geleynse, N., Storms, J.E., Walstra, D.J.R., Jagers, H.A., Wang, Z.B. & Stive, M.J. (2011) Controls on river delta formation; insights from numerical modelling. *Earth and Planetary Science Letters*, 302(1–2), 217–226.
- Goelzer, H., Nowicki, S., Payne, A., Larour, E., Seroussi, H., Lipscomb, W.H., et al. (2020) The future sea-level contribution of the Greenland ice sheet: a multi-model ensemble study of ISMIP6. *The Cryosphere*, 14(9), 3071–3096. Available from: <https://doi.org/10.5194/tc-14-3071-2020>
- Hasholt, B., Mernild, S.H., Sigsgaard, C., Elberling, B., Petersen, D., Jakobsen, B.H., et al. (2008) Hydrology and transport of sediment and solutes at Zackenberg. *Advances in Ecological Research*, 40, 197–221.
- Hasholt, B., van As, D., Mikkelsen, A.B., Mernild, S.H. & Yde, J.C. (2018) Observed sediment and solute transport from the Kangerlussuaq sector of the Greenland ice sheet (2006–2016). *Arctic, Antarctic, and Alpine Research*, 50(1), S100009. Available from: <https://doi.org/10.1080/15230430.2018.1433789>
- Hawkings, J., Wadham, J., Tranter, M., Lawson, E., Sole, A., Cowton, T., et al. (2015) The effect of warming climate on nutrient and solute export from the Greenland ice sheet. *Geochemical Perspectives Letters*, 1(1), 94–104.
- Hawkings, J., Wadham, J., Tranter, M., Telling, J., Bagshaw, E., Beaton, A., et al. (2016) The Greenland ice sheet as a hot spot of phosphorus weathering and export in the Arctic. *Global Biogeochemical Cycles*, 30(2), 191–210.
- Herman, F., De Doncker, F., Delaney, I., Prasicek, G. & Koppes, M. (2021) The impact of glaciers on mountain erosion. *Nature Reviews Earth and Environment*, 2(6), 422–435. Available from: <https://doi.org/10.1038/s43017-021-00165-9>
- Hofer, S., Tedstone, A.J., Fettweis, X. & Bamber, J.L. (2017) Decreasing cloud cover drives the recent mass loss on the Greenland ice sheet. *Science Advances*, 3(6), e1700584.
- Hoitink, A.J.F., Wang, Z.B., Vermeulen, B., Huismans, Y. & Kästner, K. (2017) Tidal controls on river delta morphology. *Nature Geoscience*, 10(9), 637–645.
- Hopwood, M.J., Carroll, D., Dunse, T., Hodson, A., Holding, J.M., Iriarte, J.L., et al. (2020) How does glacier discharge affect marine biogeochemistry and primary production in the Arctic? *The Cryosphere*, 14(4), 1347–1383.
- How, P., Messerli, A., Mätzler, E., Santoro, M., Wiesmann, A., Caduff, R., et al. (2021) Greenland-wide inventory of ice marginal lakes using a multi-method approach. *Scientific Reports*, 11(1), 4481.
- Howard, S. & Padman, L. (2021) Gr1kmTM: Greenland 1 kilometer Tide Model. Arctic Data Center, <https://doi.org/10.18739/A2251FM3S>
- Hudson, B., Overeem, I., McGrath, D., Syvitski, J.P.M., Mikkelsen, A. & Hasholt, B. (2014) MODIS observed increase in duration and spatial extent of sediment plumes in Greenland fjords. *The Cryosphere*, 8(4), 1161–1176.
- IPCC. (2021) In: Masson-Delmotte, V., Zhai, P., Pirani, A., Connors, S.L., Péan, C., Berger, S., et al. (Eds.) *Climate change 2021: the physical science basis. Contribution of working group I to the sixth assessment report of the intergovernmental panel on climate change*. Cambridge and New York, NY: Cambridge University Press.

- Irrgang, A.M., Bendixen, M., Farquharson, L.M., Baranskaya, A.V., Erikson, L.H., Gibbs, A.E., et al. (2022) Drivers, dynamics and impacts of changing Arctic coasts. *Nature Reviews Earth and Environment*, 3(1), 39–54.
- Jaeger, J.M. & Koppes, M.N. (2016) The role of the cryosphere in source-to-sink systems. *Earth-Science Reviews*, 153, 43–76.
- King, M.D., Howat, I.M., Candela, S.G., Noh, M.J., Jeong, S., Noël, B.P., et al. (2020) Dynamic ice loss from the Greenland ice sheet driven by sustained glacier retreat. *Communications Earth & Environment*, 1(1), 1–7.
- Koppes, M., Hallet, B., Rignot, E., Mouginot, J., Wellner, J.S. & Boldt, K. (2015) Observed latitudinal variations in erosion as a function of glacier dynamics. *Nature*, 526(7571), 100–103.
- Kroon, A., Abermann, J., Bendixen, M., Lund, M., Sigsgaard, C., Skov, K., et al. (2017) Deltas, freshwater discharge, and waves along the Young Sound, NE Greenland. *Ambio*, 46, 132–145.
- Kroon, A., Pedersen, J.B.T. & Sigsgaard, C. (2011) Morphodynamic evolution of two deltas in Arctic environments, East Coast of Greenland. In: *The proceedings of the Coastal Sediments 2011*, vol. 3. Singapore: World Scientific Publishing Co Pte Ltd, pp. 2299–2310.
- Lane, S.N., Bakker, M., Gabbud, C., Micheletti, N. & Saugy, J.N. (2017) Sediment export, transient landscape response and catchment-scale connectivity following rapid climate warming and Alpine glacier recession. *Geomorphology*, 277, 210–227.
- Lane, S.N. & Nienow, P.W. (2019) Decadal-scale climate forcing of alpine glacial hydrological systems. *Water Resources Research*, 55(3), 2478–2492. Available from: <https://doi.org/10.1029/2018WR024206>
- Lea, J.M. (2018) The Google Earth Engine digitisation tool (GEEDiT) and the margin change quantification tool (MaQiT)—simple tools for the rapid mapping and quantification of changing earth surface margins. *Earth Surface Dynamics*, 6(3), 551–561. Available from: <https://doi.org/10.5194/esurf-6-551-2018>
- Leggat, M.S., Owens, P.N., Stott, T.A., Forrester, B.J., Déry, S.J. & Menounos, B. (2015) Hydro-meteorological drivers and sources of suspended sediment flux in the pro-glacial zone of the retreating Castle Creek Glacier, Cariboo Mountains, British Columbia, Canada. *Earth Surface Processes and Landforms*, 40(11), 1542–1559. Available from: <https://doi.org/10.1002/esp.3755>
- Lewington, E.L., Livingstone, S.J., Clark, C.D., Sole, A.J. & Storrar, R.D. (2020) A model for interaction between conduits and surrounding hydraulically connected distributed drainage based on geomorphological evidence from Keewatin, Canada. *The Cryosphere*, 14(9), 2949–2976. Available from: <https://doi.org/10.5194/tc-14-2949-2020>
- Livingstone, S.J., Sole, A.J., Storrar, R.D., Harrison, D., Ross, N. & Bowling, J. (2019) Brief communication: subglacial lake drainage beneath Isunguata Sermia, West Greenland: geomorphic and ice dynamic effects. *The Cryosphere*, 13(10), 2789–2796. Available from: <https://doi.org/10.5194/tc-13-2789-2019>
- Mancini, D., Dietze, M., Müller, T., Jenkin, M., Miesen, F., Roncoroni, M., et al. (2023) Filtering of the signal of sediment export from a glacier by its proglacial forefield. *Geophysical Research Letters*, 50(21), e2023GL106082. Available from: <https://doi.org/10.1029/2023GL106082>
- Mankoff, K.D., Noël, B., Fettweis, X., Ahlstrøm, A.P., Colgan, W., Kondo, K., et al. (2020) Greenland liquid water discharge from 1958 through 2019. *Earth System Science Data*, 12(4), 2811–2841.
- Mao, L., Dell'Agnese, A. & Comiti, F. (2017) Sediment motion and velocity in a glacier-fed stream. *Geomorphology*, 291, 69–79.
- Meire, L., Søgaard, D.H., Mortensen, J., Meysman, F.J.R., Soetaert, K., Arendt, K.E., et al. (2015) Glacial meltwater and primary production are drivers of strong CO₂ uptake in fjord and coastal waters adjacent to the Greenland ice sheet. *Biogeosciences*, 12(8), 2347–2363.
- Mouginot, J., Rignot, E., Björk, A.A., Van den Broeke, M., Millan, R., Morlighem, M., et al. (2019) Forty-six years of Greenland ice sheet mass balance from 1972 to 2018. *Proceedings of the National Academy of Sciences*, 116(19), 9239–9244.
- Nghiem, S.V., Hall, D.K., Mote, T.L., Tedesco, M., Albert, M.R., Keegan, K., et al. (2012) The extreme melt across the Greenland ice sheet in 2012. *Geophysical Research Letters*, 39(20), 2012GL053611. Available from: <https://doi.org/10.1029/2012GL053611>
- Nielsen, N. (1994) Geomorphology of a degrading arctic delta, Sermilik, south-east Greenland. *Geografisk Tidsskrift - Danish Journal of Geography*, 94(1), 46–57.
- Nienhuis, J.H., Houtink, A.J.F. & Törnqvist, T.E. (2018) Future change to tide-influenced deltas. *Geophysical Research Letters*, 45(8), 3499–3507.
- Noël, B., van de Berg, W.J., Lhermitte, S. & van den Broeke, M.R. (2019) Rapid ablation zone expansion amplifies North Greenland mass loss. *Science Advances*, 5(9), eaaw0123. Available from: <https://doi.org/10.1126/sciadv.aaw0123>
- Orwin, J.F. & Smart, C.C. (2004) The evidence for paraglacial sedimentation and its temporal scale in the deglaciating basin of Small River Glacier, Canada. *Geomorphology*, 58(1–4), 175–202. Available from: <https://doi.org/10.1016/j.geomorph.2003.07.005>
- Overeem, I., Hudson, B.D., Syvitski, J.P., Mikkelsen, A.B., Hasholt, B., Van Den Broeke, M.R., et al. (2017) Substantial export of suspended sediment to the global oceans from glacial erosion in Greenland. *Nature Geoscience*, 10(11), 859–863.
- Overeem, I., Nienhuis, J.H. & Piliouras, A. (2022) Ice-dominated Arctic deltas. *Nature Reviews Earth and Environment*, 3(4), 225–240.
- Patton, H., Swift, D.A., Clark, C.D., Livingstone, S.J. & Cook, S.J. (2016) Distribution and characteristics of overdeepenings beneath the Greenland and Antarctic ice sheets: implications for overdeepening origin and evolution. *Quaternary Science Reviews*, 148, 128–145.
- Pedersen, J.B.T., Kroon, A., Jakobsen, B.H., Mernild, S.H., Andersen, T.J. & Andresen, C.S. (2013) Fluctuations of sediment accumulation rates in front of an Arctic delta in Greenland. *The Holocene*, 23(6), 860–868. Available from: <https://doi.org/10.1177/0959683612474480>
- Plink-Björklund, P. (2012) Effects of tides on deltaic deposition: causes and responses. *Sedimentary Geology*, 279, 107–133. Available from: <https://doi.org/10.1016/j.sedgeo.2011.07.006>
- Porter, P.R., Smart, M.J. & Irvine-Fynn, T.D. (2019) Glacial sediment stores and their reworking. In: *Geomorphology of proglacial systems*, Vol. 1. Cham: Springer, pp. 157–176. Available from: https://doi.org/10.1007/978-3-319-94184-4_10
- Rawlins, M.A., Steele, M., Holland, M.M., Adam, J.C., Cherry, J.E., Francis, J.A., et al. (2010) Analysis of the Arctic system for freshwater cycle intensification: observations and expectations. *Journal of Climate*, 23(21), 5715–5737.
- Richter, A., Rysgaard, S., Dietrich, R., Mortensen, J. & Petersen, D. (2011) Coastal tides in West Greenland derived from tide gauge records. *Ocean Dynamics*, 61(1), 39–49. Available from: <https://doi.org/10.1007/s10236-010-0341-z>
- Riihimäki, C.A., MacGregor, K.R., Anderson, R.S., Anderson, S.P. & Loso, M.G. (2005) Sediment evacuation and glacial erosion rates at a small alpine glacier. *Journal of Geophysical Research: Earth Surface*, 110(F3), 2004JF000189. Available from: <https://doi.org/10.1029/2004JF000189>
- Savi, S., Buter, A., Heckmann, T., Theule, J., Mao, L. & Comiti, F. (2023) Multi-temporal analysis of morphological changes in an Alpine proglacial area and their effect on sediment transfer. *Catena*, 220, 106701. Available from: <https://doi.org/10.1016/j.catena.2022.106701>
- Serreze, M.C. & Barry, R.G. (2011) Processes and impacts of arctic amplification: a research synthesis. *Global and Planetary Change*, 77(1–2), 85–96. Available from: <https://doi.org/10.1016/j.gloplacha.2011.03.004>
- Sharifi, S., Hendry, M.T., Macciotta, R. & Evans, T. (2022) Evaluation of filtering methods for use on high-frequency measurements of landslide displacements. *Natural Hazards and Earth System Sciences*, 22(2), 411–430. Available from: <https://doi.org/10.5194/nhess-22-411-2022>
- Shepherd, A., Ivins, E., Rignot, E., Smith, B., van den Broeke, M., Velicogna, I., et al. (2020) Mass balance of the Greenland ice sheet from 1992 to 2018. *Nature*, 579(7798), 233–239. Available from: <https://doi.org/10.1038/s41586-019-1855-2>

- Slater, T., Shepherd, A., McMillan, M., Leeson, A., Gilbert, L., Muir, A., et al. (2021) Increased variability in Greenland ice sheet runoff from satellite observations. *Nature Communications*, 12(1), 6069. Available from: <https://doi.org/10.1038/s41467-021-26229-4>
- Smith, R.W., Bianchi, T.S., Allison, M., Savage, C. & Galy, V. (2015) High rates of organic carbon burial in fjord sediments globally. *Nature Geoscience*, 8(6), 450–453. Available from: <https://doi.org/10.1038/ngeo2421>
- Swift, D.A., Nienow, P.W. & Hoey, T.B. (2005) Basal sediment evacuation by subglacial meltwater: suspended sediment transport from haut glacier d'Arolla, Switzerland. *Earth Surface Processes and Landforms*, 30(7), 867–883. Available from: <https://doi.org/10.1002/esp.1197>
- Swift, D.A., Nienow, P.W., Spedding, N. & Hoey, T.B. (2002) Geomorphic implications of subglacial drainage configuration: rates of basal sediment evacuation controlled by seasonal drainage system evolution. *Sedimentary Geology*, 149(1–3), 5–19.
- Tedesco, M. & Fettweis, X. (2020) Unprecedented atmospheric conditions (1948–2019) drive the 2019 exceptional melting season over the Greenland ice sheet. *The Cryosphere*, 14(4), 1209–1223. Available from: <https://doi.org/10.5194/tc-14-1209-2020>
- Tedesco, M., Fettweis, X., Van den Broeke, M.R., Van de Wal, R.S.W., Smeets, C.J.P.P., van de Berg, W.J., et al. (2011) The role of albedo and accumulation in the 2010 melting record in Greenland. *Environmental Research Letters*, 6(1), 014005. Available from: <https://doi.org/10.1088/1748-9326/6/1/014005>
- Vos, K., Splinter, K.D., Palomar-Vázquez, J., Pardo-Pascual, J.E., Almonacid-Caballer, J., Cabezas-Rabadán, C., et al. (2023) Benchmarking satellite-derived shoreline mapping algorithms. *Communications Earth & Environment*, 4(1), 345. Available from: <https://doi.org/10.1038/s43247-023-01001-2>
- Wicaksono, A., Wicaksono, P., Khakhim, N., Farda, N.M. & Marfai, M.A. (2018) Tidal correction effects analysis on shoreline mapping in Jepara Regency. *Journal of Applied Geospatial Information*, 2(2), 145–151. Available from: <https://doi.org/10.30871/jagi.v2i2.981>
- Young, N.E., Briner, J.P., Maurer, J. & Schaefer, J.M. (2016) ¹⁰Be measurements in bedrock constrain erosion beneath the Greenland ice sheet margin. *Geophysical Research Letters*, 43(22), 11–708. Available from: <https://doi.org/10.1002/2016GL070258>
- Zhang, T., Li, D., East, A.E., Kettner, A.J., Best, J., Ni, J., et al. (2023) Shifted sediment-transport regimes by climate change and amplified hydrological variability in cryosphere-fed rivers. *Science Advances*, 9(45), eadi5019. Available from: <https://doi.org/10.1126/sciadv.adi5019>
- Zhao, K., Wulder, M.A., Hu, T., Bright, R., Wu, Q., Qin, H., et al. (2019) Detecting change-point, trend, and seasonality in satellite time series data to track abrupt changes and nonlinear dynamics: a Bayesian ensemble algorithm. *Remote Sensing of Environment*, 232, 111181. Available from: <https://doi.org/10.1016/j.rse.2019.04.034>

How to cite this article: Crick, R., Livingstone, S.J. & Sole, A.J.

(2025) Accelerating growth of Sermilik Delta, Greenland (1987–2022), driven by increasing runoff. *Earth Surface Processes and Landforms*, 50(8), e70116. Available from: <https://doi.org/10.1002/esp.70116>